J. Min. Metall. Sect. B-Metall. 61 (3) (2025) 317 - 332

Journal of Mining and Metallurgy, Section B: Metallurgy

OXIDATION AND PROPERTY EVOLUTION OF AISI T5 STEEL UNDER VARYING HEAT TREATMENTS

Abdenour Dadou [a,*], Hamid Dilmi [a], Boudjema Bezzazi [a], Chouaib Aribi [a,b], Ismail Daoud [c]

[a] M'hamed Bougara University -Boumerdes, Faculty of Technology, Algeria
[b] Laboratory of Food, Processing, Control and Agri-Resources Valorization, Higher School of Food Science and Agri-Food Industry, Algeria
[c] University of Sciences and Technology Houari Boumediene, Laboratory of Science and Materials Engineering, Algeria

(Received 13 July 2025; Accepted 17 November 2025)

Abstract

This study evaluates the effect of heat treatment on the mechanical, tribological, and oxidation behavior of AISI T5 steel. The chemical composition was first characterized using spectroscopy and SEM. A two-year oxidation test conducted in humid and relatively dry atmospheres showed strong environmental sensitivity: in humid air, the oxidation rate reached 11.27×10^{-2} P/P_0 per month with a sharp increase after 25 days, whereas in dry air it remained below 1.35×10^{-2} P/P_0 per month, following a linear and nearly flat trend indicative of a protective oxide scale. Heat treatment significantly increased hardness from 34.15 ± 0.59 HRC (untreated) to 62.70 ± 0.66 and 60.80 ± 0.48 HRC for water and oil quenched steels, respectively. Impact strength decreased accordingly, with oil quenching offering the best hardness-toughness balance (60.8 HRC, 2.08 Kcv). Instrumented indentation confirmed substantial surface strengthening, with HIT rising to 17.39 ± 0.29 GPa (Q. Water) and 7.68 ± 0.12 GPa (Q. Oil). Under dry sliding, wear rates were reduced by 81.3% (Q. Water) and 62.5% (Q. Oil), with faster run-in in the water-quenched condition. XRD revealed tempered martensite with Fe_3W_3C/Cr_7C_3 (Q. Water) and Co_3W_3C (Q. Oil), consistent with thermal conditions. This study provides new experimental data on the effects of 15-minute austenitization followed by oil or water quenching on the properties of AISI T5 steel, highlighting its potential for process optimization.

Keywords: *AISI T5; Oxidation; Heat treatment; Hardness; Nanoindentation; Abrasion*

1. Introduction

AISI T5 steel is categorized as a high-speed steel (HSS). It is mainly used for making cutting tools such as drills, taps, milling cutters, hand saws. Also, it is used in cold forming, where high wear resistance is required. The hardness of this steel can reach 64 HRC or more [1].

Tool steels (carbon, alloy and HSS) are subjected to quenching and tempering cycles to achieve optimal combinations of strength and toughness; they are used in mechanical fixtures for cutting, forming, and blanking of materials at either ordinary or elevated temperatures [2].

There are several ways of grouping tool steels; a particularly interesting one is to classify them according to the branch of application. Tool steels can thus be divided into four classes: (1) tool steels for cold working, (2) tool steels for hot working, (3) tool steels for plastic molds, and (4) high speed steel. The HSS class has very peculiar properties, and some authors prefer to treat it separately from other tool steels [1] .

According to Seo et al., at room temperature, alloying elements such as chromium and vanadium facilitate the development of thin, stable passive oxide layers that markedly inhibit further oxidation [3]. Wielant et al. [4] demonstrated that during thermal oxidation of SAE 1010 steel at 250 °C, oxides such as Fe_3O_4 and Fe_2O_3 rapidly form and act as diffusion barriers. Although these processes occur above ambient temperature, they underscore the importance of oxide scales in reducing oxygen and metal ion diffusion, even at moderate temperatures.

Although direct experimental data under ambient conditions remain scarce, passive films are generally

Corresponding author: a.dadou@univ-boumerdes.dz

https://doi.org/10.2298/JMMB250713025D

acknowledged to provide a certain degree of protection [5-7]. However, environmental humidity may compromise their integrity by promoting hydrogen embrittlement and delayed fracturing of protective alumina layers [8]. Tool steels alloyed with W, Cr, Co, and V form complex oxides (e.g., Cr_2O_3, V_2O_5) that may similarly degrade in humid environments, affecting the long-term stability of protective scales.

According to Ziyong Hou et al. [9] and Babasafari [10], studies focusing on high-carbon steels, their characteristics, and thermal treatments remain scarce in the literature, particularly regarding their structural behavior. In general, low-carbon steels have received more attention. High-alloy tool steels are also underexplored, mainly due to their complex, multiphase microstructures, which make both experimental investigations and modeling more challenging. Their limited application in critical energy systems reduces research prioritization, while long-term testing under real-world conditions remains time-consuming and costly [11].

One of the closest studies on this subject is by Virendra Kumar et al. [12]. It addresses the improvement of the mechanical properties of tool steels for cold working through various heat treatment processes, achieving an optimal combination of hardness and toughness by altering the microstructure. Similar findings were reported by Bo Jiang et al. [11], even after very long tempering processes [13]. According to Ashish Bhateja et al. [14], heat treatment is often associated with increasing the strength of the material; however, it can also be used to improve certain characteristics at the expense of others by adjusting treatment parameters, or to modify manufacturability objectives such as enhancing machinability. It is also a means of recovering properties like ductility after cold working operations.

This study investigates the long-term oxidation behavior of AISI T5 high speed tool steel after two years of exposure in two real atmospheric conditions: humid air and relatively dry air. In parallel, a heat treatment is applied to separate specimens, which are then subjected to a combination of destructive and non-destructive analyses. The primary objective is to assess and compare the steel's surface chemical characteristics resulting from the atmospheric exposure, as well as its mechanical performance and tribological behavior following heat treatment in two different cooling media. The goal is to identify the cooling medium that best ensures a balance of properties suited to specific operational requirements. This work provides valuable insights into high-carbon, highly alloyed tool steels and enhances existing data related to their long-term atmospheric degradation. In addition to the scientific objectives, this study also addresses an economic concern by reducing the austenitizing holding time from the typical 30 minutes to 15 minutes. The aim is to maintain comparable mechanical and tribological performance while optimizing processing time and energy consumption. This approach seeks to improve cost-efficiency without compromising material properties.

2. Materials and methods

2.1. Materials

The material used in this study is AISI T5, an iron-based alloy containing tungsten, cobalt, chromium, and vanadium. AISI T5 is classified as high-speed tool steel. The letter "T" indicates this class according to ASTM and SAE standards [15, 16]. This designation reflects its characteristics: controlled high tungsten content along with other alloying elements. The number (5) refers to its sequential and historical classification [2].

2.1.1. Spectroscopy

The chemical composition of AISI T5 steel was determined using an optical emission spectrometer (SPECTROMAXx, AMETEK). This equipment provides precise quantitative analysis of metallic elements in steels and alloys. The table 1 presents the chemical composition obtained from this spectroscopy analysis.

2.1.2. Scanning Electron Microscope (SEM)

Microscopic observations were conducted using a Zeiss Gemini 300 scanning electron microscope (SEM), which is equipped with an integrated Oxford EDS (Energy Dispersive X-ray Spectroscopy) detector, allowing simultaneous microstructural imaging and elemental analysis. EDS analysis verified the presence of alloying elements per ASTM A600, with some variation in the measured percentages. Although suitable for elemental identification, EDS is less accurate for quantification due to factors such as surface roughness, matrix effects, and detector sensitivity [17, 18].

2.2. Experimental procedures

2.2.1. Machining and Polishing

The samples are prepared as pellets, 6 mm thick and 25.4 mm in diameter, with dimensions determined by the specific requirements of testing equipment such as X-ray diffractometers, scanning electron microscopes (SEM), tribometers, and nanoindenters. Machining is performed using conventional DAINITCHI lathes. All samples

Table 1. *Chemical composition (in weight %)*

Element	Fe	C	W	Co	Cr	V	Mo	Ta	Si	Ni	Mn	Cu	Others
Analyze	63.9	0.77	18.15	8.57	4.15	1.37	0.64	0.56	0.405	0.281	0.277	0.195	0.731

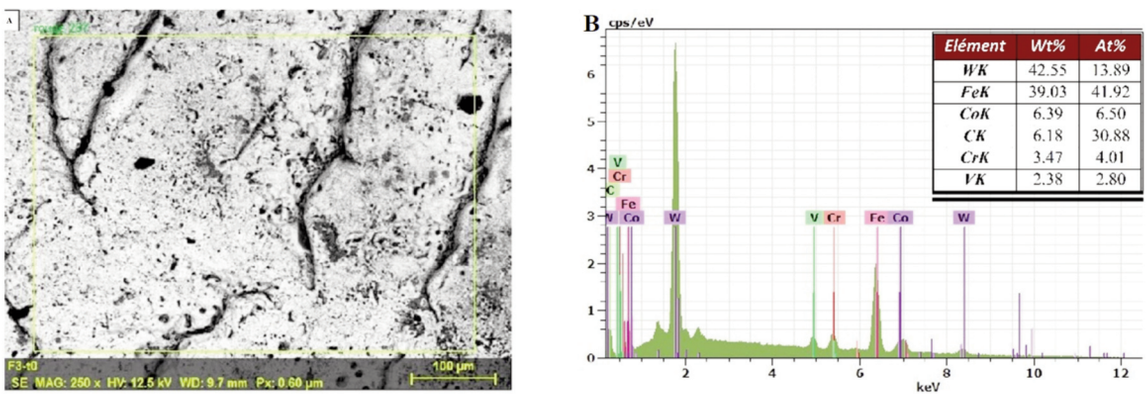

Figure 1. *SEM analysis: A) Secondary electron image (500x); B) Elemental chemical analysis*

undergo advanced mechanical polishing to obtain a mirror-polished surface.

2.2.2. Oxidation Experience

Two AISI T5 steel samples were used in this experiment. The first sample, weighing 25.9609 g, was exposed to indoor air in a closed laboratory, while the second sample, weighing 25.4661 g, was exposed to outdoor air, approximately one kilometer from the Mediterranean Sea. The initial weight (P_0) of each sample was recorded prior to the start of the experiment. At regular intervals, the samples were reweighed, and their new weights (P) were recorded. The weight change ($\Delta P = P\text{-}P_0$), corresponding to oxidation over time, was determined for each sample.

The oxidation rate, defined as the ratio between the weight change and the initial weight, was also calculated. Atmospheric and indoor relative humidity levels were measured daily using a PCE-313A hygrometer, and the average humidity was computed for each weighing interval.

The experiment lasted two years: weighings were performed weekly during the first year and monthly during the second year. Finally, the oxidation behavior of the steel was compared between the humid outdoor environment and the relatively dry indoor environment. The experiment began in the first week of May.

2.2.3. Heat Treatment Cycle

The heat treatment was performed in a STUART electric furnace with a heating rate of 10 °C/min. The austenitizing holding time was set to 15 min for the 6 mm thick samples, reduced from the typical 30 min. Tempering was performed at 300 °C for a duration of

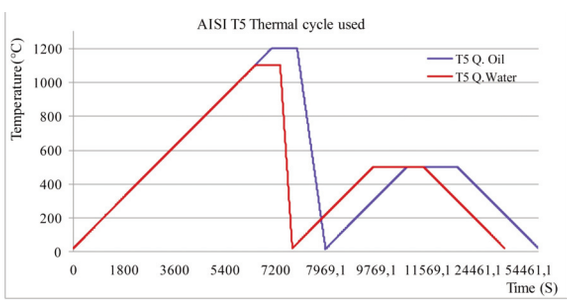

Figure 2. *Applied thermal cycle*

30 min, corresponding to 300 s/mm. Cooling rates were 150 °C/s in lukewarm water and 70 °C/s in oil [19], The complete thermal cycle applied to the samples is presented in Figure 2.

The following points are indicated on the heat treatment cycle graph for quenching and tempering: start of heating, start of holding, and start and end of cooling. To keep the graph clear, representative, and uncluttered, half of the x-axis, which represents the quenching heat treatment, was assigned approximately 8000 seconds, while the other half, representing tempering, was assigned approximately 45000 seconds. The two curves are identical except for the cooling segment during quenching, where the slopes differ due to the varying cooling rates.

2.2.4. Hardness Test

The Rockwell hardness (HRC) test was conducted using a NEWAGE VERSITRON apparatus under a 30 N load applied for 10 seconds. For each condition, at least five indentations were performed to ensure reproducibility, and the average value was reported. These measurements provide a quantitative evaluation of the bulk material's resistance to plastic

deformation, thereby allowing an accurate assessment of the heat treatment efficiency in achieving the targeted high-hardness state.

2.2.5. Resilience Test

The impact toughness of the studied steel was evaluated using the Charpy V-notch test according to the ASTM E23 and ISO 148-1 standards. Standard rectangular specimens (55 × 10 × 10 mm^3) with a V-shaped notch of 2 mm depth and a 45° angle were prepared along the longitudinal direction of the samples. The tests were carried out using an instrumented pendulum impact tester at room temperature. The absorbed energy (in joules) was recorded directly from the equipment, representing the material's ability to resist fracture under dynamic loading.

2.2.6. Nanoindentation

Nanoindentation was performed according to the Oliver and Pharr method using a Berkovich indenter (AE TTX device), with a loading/unloading rate of 1000 mN/min, a hold time of 10 seconds, and a maximum applied load of 500 mN. For each condition - untreated, water-quenched, and oil-quenched - two indentations are performed to ensure measurement reliability, account for microstructural heterogeneity, and reduce the influence of local surface defects. The results used are the microhardness $HV_{0.5}$, the indentation hardness HIT, defined as the ratio of the applied force to the projected contact area, and the Young's modulus E, in accordance with the NF EN ISO 14577 standard. The range used is: micro-interval, 2 > F; h > 0.2 µm [20]. A comparison will be made between the data obtained from the untreated sample and from the samples exposed to each cooling environment.

2.2.7. Tribology

Friction and wear tests without lubrication were conducted using a Pin-On-Disc and Oscillating TRIBO Tester (Tt TRIBOtechnic) in rotary mode. A 6 mm diameter alumina ball (Al_2O_3), replaced after each test, served as the counter-body. Tests were performed under a normal load of 11 N, at a sliding speed of 200 mm/s, with a wear track radius of 8 mm and a total sliding distance of 150 m. Experiments were carried out in ambient air at ~25.9 °C and 44% relative humidity.

Three samples were evaluated: as-received, water-quenched, and oil-quenched. Wear was assessed by mass loss, and the coefficient of friction was continuously recorded. Worn surfaces were analyzed using 2D and 3D profilometry to evaluate the wear track topography. For each sample, four profilometric scans were performed under identical conditions, with 307,200 measurement points per scan. Roughness parameters (Ra, Rp, Rq, Rt, Rv) were extracted, and wear track dimensions (ΔX and ΔZ in X and Y directions) were estimated using Image J software. This combined approach enabled a detailed quantitative assessment of wear morphology, complementing the tribological analysis.

2.2.8. XRD analysis

The X-ray diffraction (XRD) analysis was carried out using a reflection–transmission spinner on an EMPYREAN diffractometer equipped with Cu K_α radiation (λ = 1.54060 A°). The scans were performed in continuous mode with a step size of 0.0130° over a 2θ range up to 120°, at room temperature (25 °C). The HighScore Plus software was employed to identify the nature of the various microstructural phases. This characterization technique enabled the identification of the matrix type and the carbides present in the microstructure of the analyzed samples, as well as the phase transformations that occurred after quenching in the two different cooling media.

3. Results and discussion

3.1. Oxidation Study

The oxidation behavior of AISI T5 steel was monitored over a period of two years under both humid and dry atmospheric conditions. Figure 3 clearly shows a significantly higher weight gain in humid conditions compared to dry ones. This difference becomes more pronounced over time, indicating a strong environmental influence on oxidation kinetics.

According to Table 2, the monthly mass gain in humid conditions increases rapidly, especially during the second year. In the first year, the weight gains rise

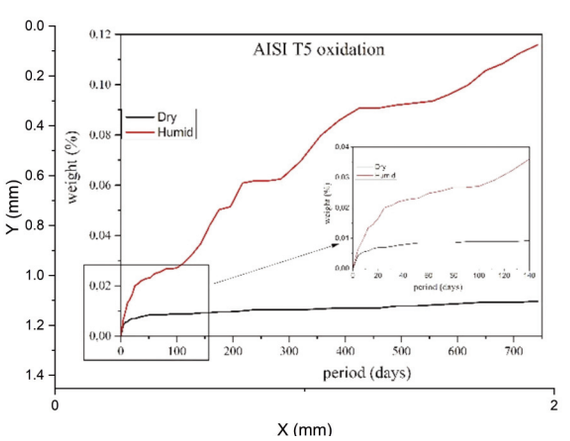

Figure 3. *Oxidation behavior of AISI T5 steel in dry and humid conditions*

Table 2. *Mass gain per month (10^{-2} g)*

Env.	Year	May	June	July	Aug.	Sept.	Oct.	Nov.	Dec.	Jan.	Feb.	Mar.	April
Humid	First	0.42	0.59	0.68	0.74	0.94	1.28	1.31	1.57	1.57	1.59	1.77	2.03
	Second year	2.09	2.19	2.31	2.31	2.34	2.36	2.38	2.45	2.54	2.69	2.76	2.87
Dry	First	0.18	0.22	0.22	0.23	0.24	0.25	0.25	0.27	0.27	0.27	0.27	0.28
	Second year	0.28	0.29	0.29	0.29	0.31	0.31	0.32	0.33	0.34	0.35	0.35	0.35

Table 3. *Oxidation rate percent per month ($(\Delta P/ P_0) \times 10^2$)*

Env.	Year	May	June	July	Aug.	Sept.	Oct.	Nov.	Dec.	Jan.	Feb.	Mar.	April
Humid	First	1.649	2.317	2.67	2.906	3.691	5.026	5.144	6.165	6.165	6.244	6.95	7.971
	Second	8.206	8.6	9.071	9.071	9.189	9.267	9.346	9.621	9.974	10.563	10.838	11.27
Dry	First	0.693	0.847	0.847	0.886	0.924	0.963	0.963	1.04	1.04	1.04	1.04	1.079
	Second	1.079	1.117	1.117	1.117	1.194	1.194	1.233	1.271	1.31	1.348	1.348	1.348

from 0.42×10^{-2} g in May to 2.03×10^{-2} g by April. The second year shows an even more aggressive progression, reaching 2.87×10^{-2} g by the following April. This cumulative trend supports the visual progression seen in Figure 3, where the humid curve steeply rises after the first 25 days.

In contrast, dry conditions exhibit a much slower oxidation progression, and the greatest mass gain rate occurs during the first week (approximately 5 days). The first-year values range from 0.18×10^{-2} g to only 0.28×10^{-2} g and the second year shows a marginal increase, peaking at 0.35×10^{-2} g. The slope of the dry-condition curve remains nearly linear and flat throughout the period, suggesting the formation of a stable and protective oxide layer that limits further oxidation. According to [21], the authors examined the formation mechanism of chromium-rich protective oxide layers on hot-work tool steel, which are comparable to those formed on AISI T5 steel due to their chromium content. The isothermal oxidation behavior of X38CrMoV5 steel was studied at 600 °C and 700 °C under both dry and humid atmospheres. Their results demonstrated that the formation of a Cr_2O_3-rich protective oxide layer effectively limits oxidation, confirming the role of chromium in enhancing oxidation resistance.

To further quantify this behavior, Table 3 presents the monthly oxidation rate ($\Delta P\times100/P_0$).

Table 3 provides insights into the oxidation rate. In humid air, the rate changes from 1.65×10^{-2} % in May to over 11×10^{-2} % by the end of the second year, confirming accelerated degradation. The sharp increases in October and November of the first year (5.026×10^{-2} and 5.144×10^{-2} %, respectively) likely reflect seasonal humidity peaks. A similar trend continues in the second year with oxidation rates reaching 11.27×10^{-2} %. In dry conditions, the oxidation rate remains almost constant, never exceeding 1.35×10^{-2} % per month. This suggests that oxidation is controlled and likely governed by diffusion through a protective oxide layer, limiting mass gain. The inset in Figure 3, zooming into the first 140 days, emphasizes the initial rapid weight gain in humid air, a phenomenon not observed under dry conditions. This reflects early-stage oxide layer instability in humid environments, leading to more aggressive corrosion.

AISI T5 steel demonstrates good oxidation resistance in dry air, but is significantly more susceptible to oxidation in humid conditions, especially over long durations. The data support the conclusion that humidity accelerates oxidation through continuous oxide growth, likely due to moisture-assisted breakdown of protective layers [22].

3.2. Impact on Mechanical Properties

3.2.1. Results of the Rockwell Hardness Measurements

The Table 4 shows the obtained Rockwell hardness results. The untreated steel exhibited a relatively low Rockwell hardness of 34.15 ± 0.59 HRC. After heat treatment, a significant improvement in hardness was observed. Water quenching from 1100 °C produced the highest hardness value (62.70 ± 0.66 HRC), whereas oil quenching from 1200 °C yielded a slightly lower hardness (60.80 ± 0.48 HRC) (Table 4).The superior hardness achieved through water quenching, despite a 100 °C lower austenitizing temperature, highlights the critical influence of a higher cooling rate in promoting martensite formation [23]. The difference in cooling rates between the two quenching media is further reflected in the hardness variability. Oil quenching exhibited a lower standard

Table 4. *Hardness Rockwell obtained*

Sample	HRC
Untreated	34.15 ± 0.59
Q. Water	62.70 ± 0.66
Q. Oil	60.80 ± 0.48

deviation (± 0.48 HRC) compared to water quenching (± 0.66 HRC), indicating a more uniform hardness distribution. This can be attributed to the moderate cooling rate of oil, which allows a more controlled phase transformation and minimizes internal stresses. Conversely, the rapid cooling associated with water quenching can induce microstructural heterogeneity, resulting in a wider spread of hardness values. Overall, both quenching methods substantially increased hardness compared with the untreated steel. However, while water quenching provides higher hardness, oil quenching offers greater uniformity and consistency, which may be advantageous for applications requiring homogeneous mechanical properties. Consequently, the selection of the quenching medium should balance the desired hardness level with the acceptable degree of variability in the material's properties. It is also noteworthy that several attempts at heat treatment at 1200 °C followed by water quenching were unsuccessful, as the specimens developed cracks (Figure 4). This observation suggests that the steel loses considerable toughness when quenched from high austenitizing temperatures in water. Further investigation will be conducted to better understand the relationship between austenitizing temperature, cooling rate, and the resulting brittleness.

Figure 4. *Effect of water quenching after heating AISI T5 to 1200 °C*

3.2.2. Results of the Impact Toughness Measurements

The measured resilience values (Table 5) indicate that the investigated steel is very hard, exhibiting one of the lowest impact toughness levels typically observed in steels. The untreated steel displays an impact toughness of 2.20 ± 0.26 Kcv. Following heat treatment, oil quenching slightly decreases this value to 2.08 ± 0.16 Kcv (-5.5 %). This minor reduction may result from several factors: an insufficient austenitizing temperature and/or holding time, which could prevent complete dissolution of carbides; the presence of undissolved carbides, which lowers the carbon content of the matrix and consequently produces softer martensite; and possible surface decarburization if the furnace atmosphere was not inert. Additionally, the presence of retained austenite in this steel grade could also contribute to the reduced toughness. In contrast, water quenching leads to a significant decrease in toughness, reducing the impact energy to 1.08 ± 0.13 Kcv (-50%). This drastic reduction can be attributed to the formation of a predominantly martensitic and brittle microstructure [24]. The lower scatter observed for oil quenching (± 0.16) compared to both the untreated (± 0.26) and water-quenched states (± 0.17) further supports the greater uniformity and stability of mechanical properties obtained with oil quenching. Overall, these results confirm that while both quenching methods increase hardness, they do so at the expense of toughness. The trade-off between hardness and impact resistance must therefore be carefully considered when selecting the quenching medium, depending on the intended application and service conditions.

Table 5. *Resilience results*

Sample	Kcv
Untreated	2.20 ± 0.26
Q. Water	1.08 ± 0.13
Q. Oil	2.08 ± 0.16

3.2.3. Hardness as a Function of Toughness

Among the various heat treatment conditions evaluated, oil quenching yielded the most favorable compromise between hardness and toughness. A Rockwell hardness of 60.8 HRC was obtained along with an impact toughness of 2.08 Kcv, indicating an effective synergy between surface resistance and energy absorption capacity. In contrast, water

quenching produced a slightly higher hardness of 62.7 HRC but significantly reduced toughness (1.10 Kcv), suggesting a trade-off that could restrict its use in applications where impact resistance is critical. As illustrated in Figure 5, the selected oil-quenching parameters enabled a desirable balance of mechanical properties. This balance is particularly advantageous in-service conditions involving both abrasive wear and mechanical shocks. The results confirm that the heat treatment route adopted enhances hardness while preserving adequate toughness, supporting its suitability for demanding tooling applications.

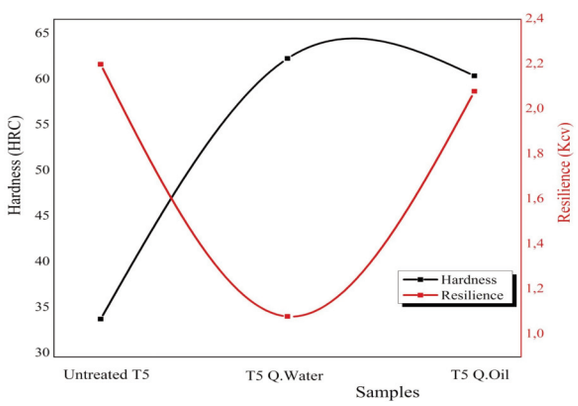

Figure 5. *Hardness as a function of Toughness for AISI T5 steel*

3.2.4. Nanoindentation Measurements

The load–unload curves and the indentations produced by the indenter during the two tests are shown in Figure 6. The results of the nanoindentation test are summarized in Table 6.

3.2.4.1. Indentation Hardness Measurements (HIT)

As illustrated in Figure 6 (imprint images), the untreated sample, represented by the black curve, exhibits the largest indentation area. The oil-quenched sample (blue) displays a moderately smaller imprint, whereas the water-quenched sample (red) shows the smallest one, indicating a higher hardness.

According to the x-axis data, indentation depths range from approximately 1.67 to 1.70 µm for the water-quenched condition (standard deviation ≈ 0.0212 µm), 1.83 to 1.84 µm for the oil-quenched condition (standard deviation ≈ 0.0071 µm), and 2.29 to 2.40 µm for the untreated material (standard deviation ≈ 0.0778 µm). These standard deviation values reflect the relative homogeneity of each condition: the oil-quenched sample exhibits the most uniform response to indentation, indicating a more homogeneous microstructure. In contrast, the untreated material shows the highest variability, suggesting greater heterogeneity due to the absence of thermal processing. The water-quenched condition falls between the two, displaying moderate variability. As with imprint width, indentation depth provides insight into surface mechanical properties, particularly hardness. The nanoindentation results clearly highlight the significant influence of heat treatment on the mechanical response of the material.

The untreated specimen exhibited the lowest hardness (4.11 ± 0.27 GPa), corresponding to a likely ferrite-pearlite microstructure. Water quenching resulted in the highest hardness (17.39 ± 0.29 GPa), indicative of a predominantly martensitic structure due to the rapid cooling rate. This represents an increase of approximately 323% compared to the

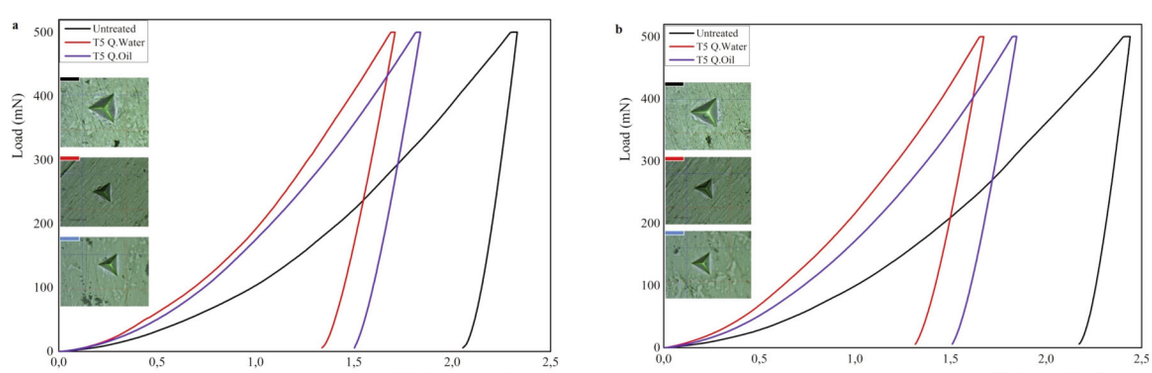

Figure 6. *Load–unload curves and surface indentations, a) First indentation test; b) Second indentation test*

Table 6. *Summary of nanoindentation test results*

Sample	HIT (GPa)	$HV_{0.5}$	YOUNG Modulus (GPa)
Untreated	4.11±0.27	381.18±25.26	219.35±11.16
Q. Water	17.39±0.29	1610.65±26.79	392.21±41.78
Q. Oil	7.68±0.12	710.83±11.23	221.96±4.43

untreated state [25]. Oil quenching led to intermediate hardness (7.68 ± 0.12 GPa), suggesting partial martensite formation alongside other transformation products such as bainite or retained austenite [26]. This corresponds to a 87% increase in hardness relative to the untreated sample. The lower standard deviation in oil-quenched samples reflects greater homogeneity in the resulting microstructure. These results highlight the critical role of quenching media in tailoring hardness through microstructural transformations.

3.2.4.2. Micro hardness $HV_{0.5}$

The Vickers microhardness measurements ($HV_{0.5}$) reveal a pronounced influence of heat treatment on the mechanical response of the investigated steel. The untreated sample exhibited the lowest hardness value (381.18 ± 25.26 $HV_{0.5}$), consistent with the ferrite–pearlite microstructure typically observed in annealed steels. This relatively soft condition serves as a reference for assessing the effectiveness of the subsequent heat treatments. The water-quenched sample showed a remarkable increase in hardness, reaching 1610.65 ± 26.79 $HV_{0.5}$ - an enhancement of approximately 323% compared with the untreated state. This substantial rise in hardness can be attributed to the formation of a predominantly martensitic microstructure, resulting from the rapid cooling rate during quenching [25]. The relatively low standard deviation indicates good reproducibility and microstructural uniformity.

In contrast, the oil-quenched sample attained an intermediate hardness of 710.83 ± 11.23 $HV_{0.5}$, corresponding to an increase of about 87% over the untreated condition. This suggests the development of a mixed microstructure, likely comprising partial martensite together with bainite and/or retained austenite, owing to the slower cooling rate of oil quenching [26]. Notably, this sample exhibited the lowest standard deviation, indicating excellent homogeneity in the hardness distribution.

Overall, these findings clearly demonstrate that the quenching medium exerts a significant effect on the hardness by controlling the nature and extent of microstructural transformations. Water quenching yields the highest hardness but may induce internal stresses and brittleness, whereas oil quenching provides a more balanced combination of hardness and structural integrity.

3.2.4.3. Determination of Young's Modulus

The Young's modulus measurements reveal a pronounced influence of heat treatment on the stiffness of the investigated steel. The untreated sample exhibited a Young's modulus of 219.35 ± 11.16 GPa, which is characteristic of an annealed ferrite–pearlite microstructure, reflecting moderate elasticity. Following water quenching, the Young's modulus increased markedly to 392.21 ± 41.78 GPa, representing an enhancement of approximately 79% compared to the untreated condition. This significant increase can be attributed to the formation of a predominantly martensitic microstructure [24], which imparts greater stiffness. However, the relatively high standard deviation (± 41.78) indicates reduced uniformity in stiffness distribution, likely due to internal stresses induced by the rapid cooling process. In contrast, the oil-quenched sample displayed a Young's modulus of 221.96 ± 4.43 GPa, nearly identical to that of the untreated specimen, with only a 1.2% increase. This suggests minimal variation in stiffness, likely associated with the partial transformation to martensite combined with other phases such as bainite [26]. The notably lower standard deviation (± 4.43) reflects a more homogeneous stiffness distribution than that observed in the water-quenched condition.

Overall, water quenching produces a substantial increase in Young's modulus but introduces greater variability due to the development of internal stresses, whereas oil quenching yields a more uniform, albeit modest, improvement in stiffness.

These results emphasize the critical role of the quenching medium in balancing stiffness enhancement, structural uniformity, and microstructural transformation. Specifically, oil quenching offers a favorable compromise between stiffness control and toughness retention, while water quenching maximizes rigidity at the expense of increased brittleness.

3.2.5. Comparative Study between Rockwell hardness and Vickers microhardness measurements

The hardness values obtained from both Rockwell (HRC) and Vickers microhardness ($HV_{0.5}$) consistently demonstrate the impact of different quenching treatments on the steel's mechanical properties. The untreated sample shows a low hardness of 34.15 ± 0.59 HRC, which increases significantly after water quenching (62.70 ± 0.66 HRC) and oil quenching (60.80 ± 0.48 HRC). The corresponding Vickers microhardness values show a similar trend, with the untreated sample at 381.18 ± 25.26 $HV_{0.5}$, increasing dramatically to 1610.65 ± 26.79 $HV_{0.5}$ for water quenching and 710.83 ± 11.23 $HV_{0.5}$ for oil quenching.

These results reinforce the finding that water quenching yields the highest hardness, followed by oil quenching. The significant increase in microhardness, especially with water quenching, highlights the

substantial effect of the cooling rate on the steel's mechanical properties.

3.3. Tribological Studies

Results of the abrasion test are presented in Table 7 and Figure 7.

Table 7. *Coefficients of friction and wear rates ($mm^3/N\times m$)*

Sample	Friction coefficient	Wear rate (10^{-5})
Untreated	0.62	11.4
Q. Water	0.7728	2.13
Q. Oil	0.7094	4.27

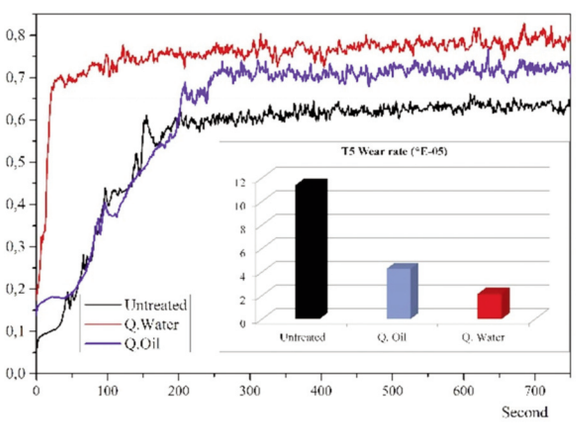

Figure 7. *Friction Coefficient and wear rate of AISI T5*

Figure 7 shows that the surface composition significantly influences the friction and wear behavior in hard materials such as AISI T5. In the water-quenched condition, a steady-state friction regime is reached rapidly, within approximately 25 seconds. In contrast, for the untreated and oil-quenched AISI T5 samples, this steady-state is established only after about 200 seconds. This delay can be explained by the lower surface hardness of the untreated and oil-quenched samples, which extends the running-in period through several combined mechanisms: increased plastic deformation, generation of larger wear debris (which delays the formation of protective tribofilms), progressive work hardening, and a more ductile microstructure that facilitates contact "softening" [27, 28].

Conversely, the water-quenched sample, characterized by a higher surface hardness, promotes faster mechanical stabilization of the contact and the development of adherent protective films, allowing the system to reach steady-state conditions more quickly. These findings are consistent with previous tribological studies on alloyed steels and confirm that surface hardness and microstructural features play a key role in governing the running-in kinetics under friction conditions [28-30].

3.3.1. Determination of the Coefficient of Friction

The coefficient of friction reflects a material's resistance to abrasion. In this study, water quenching yielded the most wear-resistant surface, followed by oil quenching. Table 7 presents the results obtained from the abrasion test, recorded after 200 seconds once a steady state was established.

The friction coefficient of the untreated sample is 0.62. After oil quenching, it increases to 0.7094, a rise of approximately 0.09 or 14.5%. Water quenching leads to a further increase to 0.7728, corresponding to a 24.6% increase.

As clearly illustrated in Figure 7, the red curve lies above the blue one, which in turn lies above the black curve.

3.3.2. Determination of Wear Rate

The wear rate results are presented in Table 7. The water-quenched steel exhibits the lowest value: 2.13×10^{-5} $mm^3/N\times m$, compared to 4.27×10^{-5} $mm^3/N\times m$ for the oil-quenched one-approximately half.

Compared to the untreated sample, this parameter is significantly improved by heat treatment, enhancing the steel's wear resistance. Under the applied experimental conditions, the amount of material removed decreases by 7.13×10^{-5} $mm^3/N\times m$ (62.54%) with oil quenching and by 9.27×10^{-5} $mm^3/N\times m$ (81.3%) with water quenching.

The latter cooling medium provides the best wear resistance. This performance is achieved without overlooking the benefit of the 100 °C reduction in the austenitizing, resulting from the adopted water quenching parameters.

3.3.3. 2D/3D Profilometric Characterization of the Worn Surface

The surface roughness data obtained from the profilometer is given in table 8. Table 9 presents the estimated dimensional parameters and wear volume derived from Image J analysis, including ΔX, ΔZ (for both X and Y profiles), the approximate cross-sectional area, and the estimated groove volume.

3.3.3.1. Surface Topography of the Untreated AISI T5 Sample

The surface analysis of four different wear zones on the untreated AISI T5 steel revealed a consistently rough and irregular topography, attributed to the absence of any thermal or mechanical treatment. The arithmetic average roughness (Ra) ranged from 1.877 µm to 2.4 µm, with a mean value of 2.06 ± 0.25 µm, indicating a moderately high variability in

Table 8. *Surface roughness parameters provided by the profilometer*

	Untreated T5	AISI T5 Q. Water	AISI T5 Q. Oil
Mean surface height (Z)	0.20 ± 0.01	0.12 ± 0.02	0.22 ± 0.13
Ra (average roughness)	2.06 ± 0.25	1.60 ± 0.04	1.78 ± 0.34
Rq (root mean square roughness)	3.35 ± 0.48	2.78 ± 0.10	3.00 ± 0.59
Rp (maximum profile peak height)	8.71 ± 2.23	8.58 ± 0.22	8.71 ± 1.88
Rv (maximum profile valley depth)	-11.20 ± 0.44	-9.55 ± 0.21	-8.74 ± 2.22
Rt (total height of the profile)	19.91 ± 1.99	18.13 ± 0.39	17.45 ± 4.10

Table 9. *Dimensional parameters and wear volume estimation from Image J (ΔX, ΔZ, area, volume)*

	Untreated T5	AISI T5 Q. Water	AISI T5 Q. Oil
ΔX (profil X)	567.71	567.71	567.72
ΔZ (profil X)	0.23	0.18	0.21
ΔX (profil Y)	69.46	92.85	95.6
ΔZ (profil Y)	15.75	9.18	9.65
Area (groove cross-section)	758.55	721.45	664.4
volume (groove) × 10^5	4.3	4.08	3.77

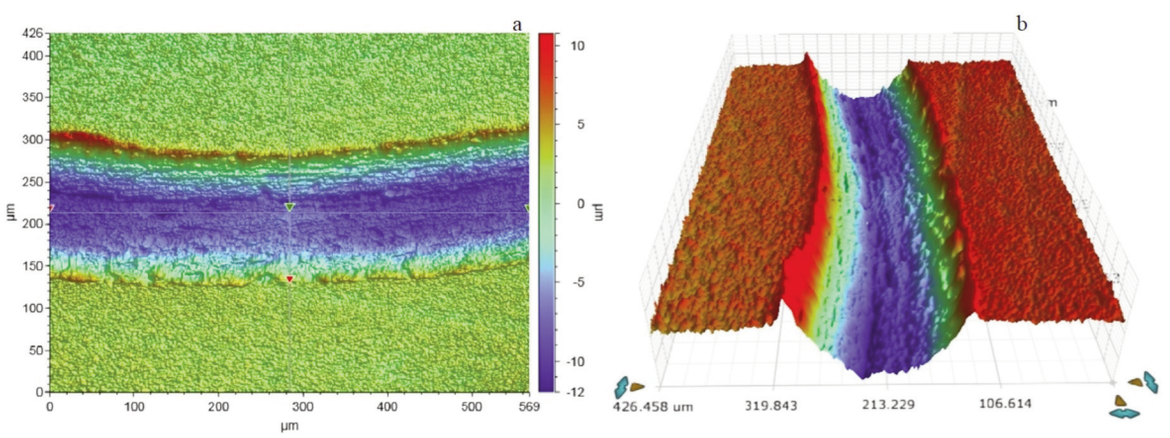

Figure 8. *Surface topography of the wear track on untreated AISI T5 steel after dry sliding test, a) 2D View with Profiles, b) 3D View with Profiles*

surface texture. The total profile height (Rt) showed values between 18.243 µm and 22.3 µm, with a mean of 19.91 ± 1.99 µm, reflecting significant surface deformation across the wear zones. The maximum valley depth (Rv) averaged –11.20 ± 0.44 µm, showing relatively low dispersion and suggesting consistent groove formation in the wear tracks. Other roughness parameters such as Rq (3.35 ± 0.48 µm) and Rp (8.71 ± 2.23 µm) also support the observation of a rough, uneven surface profile. All 3D profilometric maps revealed pronounced central grooves with asymmetric flanks and lateral roughness, characteristic of wear dominated by adhesive and abrasive mechanisms [31]. These features are consistent with the tribological performance of the untreated steel, which exhibited a relatively high coefficient of friction (0.6200) and a significant wear rate (11.4 × 10^{-5} $mm^3/N\times m$), confirming its poor resistance to dry sliding conditions.

Dimensional analysis of the wear groove using Image J further quantified the damage: the groove width and depth reached ΔX = 567.71 µm, ΔZ = 0.23 µm along the X-profile and ΔX = 69.46 µm, ΔZ = 15.75 µm along the Y-profile. The estimated cross-sectional area of the groove was 758.55 μm^2, corresponding to an estimated wear volume of 4.30 × 10^5 μm^3, supporting the profilometric and tribological findings regarding the severity of the wear process in the untreated condition.

3.3.3.2. Surface Topography of the Water-Quenched AISI T5 Sample

The surface analysis of four wear zones on the heat-treated and water-quenched AISI T5 steel revealed a more regular and mechanically stabilized topography, consistent with a uniform martensitic transformation induced by quenching [32]. The arithmetic average roughness (Ra) values ranged from

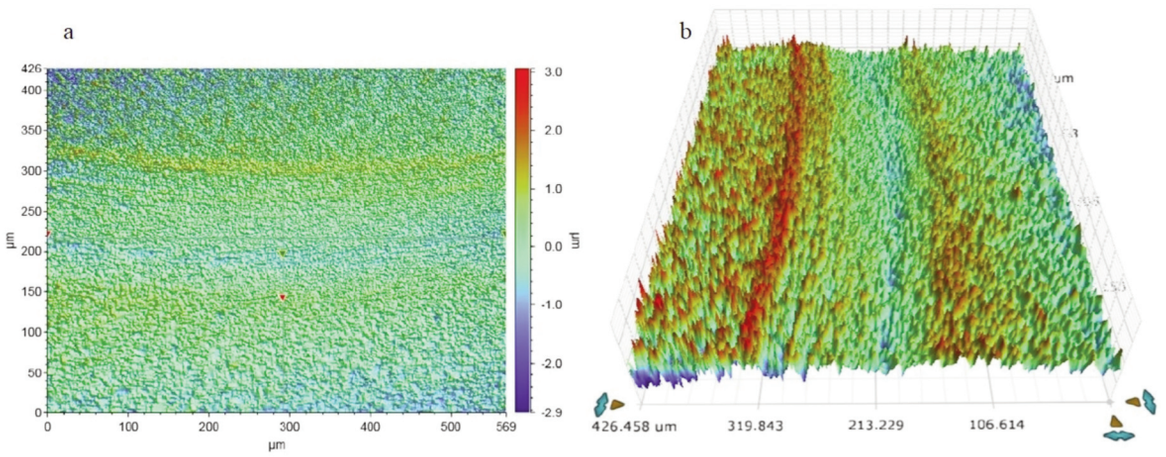

Figure 9. *Surface topography of the wear track on AISI T5 Q- Water steel after dry sliding test, (a) 2D height map with X and Y surface profiles and roughness parameters, (b) 3D perspective view showing the depth and morphology of the wear scar*

1.55 µm to 1.65 µm, with a mean of 1.60 ± 0.04 µm, indicating low variability and suggesting a homogeneous surface finish across the worn zones. The total profile height (Rt) varied between 17.8 µm and 18.7 µm, with a mean of 18.13 ± 0.39 µm, and the maximum valley depth (Rv) reached an average of –9.55 ± 0.21 µm, both showing limited dispersion. These low standard deviations reflect a stable and uniformly modified surface due to the heat treatment. The 3D profilometric mappings consistently showed a regular wear pattern characterized by a softened central groove and reduced surface asperities. These features are indicative of the beneficial effects of water quenching, which promoted a refined surface morphology and reduced the severity of abrasive features compared to the untreated condition [33]. Despite a relatively high coefficient of friction (0.7728), the wear rate was significantly reduced (2.13×10^{-5} mm^3/N×m), highlighting the improvement in wear resistance due to the martensitic microstructure. This enhanced performance is further supported by dimensional analysis from Image J, which revealed a groove width and depth of ΔX = 567.71 µm, ΔZ = 0.18 µm along the X-profile and ΔX = 92.85 µm, ΔZ = 9.18 µm along the Y-profile. The estimated cross-sectional area of the groove was 721.45 µm^2, corresponding to an estimated wear volume of 4.08×10^5 µm^3. These results confirm that water quenching effectively reduces material loss under dry sliding conditions while maintaining structural integrity.

3.3.3.3. Surface Topography of the Oil-Quenched AISI T5 Sample

The surface analysis of four wear zones on heat-treated and oil-quenched AISI T5 steel revealed a more heterogeneous and irregular topography, indicative of a less uniform martensitic transformation compared to water quenching [33]. The arithmetic average roughness (Ra) varied from 1.30 µm to 2.09 µm, with a mean of 1.78 ± 0.34 µm, reflecting a relatively high surface variability. Similarly, the total profile height (Rt) showed a wide range from 11.5 µm to 20.3 µm, with an average of 17.45 ± 4.10 µm, and the maximum valley depth (Rv) reached an average of –8.74 ± 2.22 µm, highlighting the inconsistent depth and morphology of the wear tracks. The elevated standard deviations across these roughness parameters underscore the inhomogeneous nature of the surface, likely caused by non-uniform thermal gradients during the oil quenching process.

3D profilometric mappings confirmed the presence of deeper and more erratic grooves, as well as pronounced valleys, contributing to increased topographical heterogeneity. This irregularity in the surface texture is associated with a lower coefficient of friction (0.7094) compared to water quenching, but a significantly higher wear rate of 4.27×10^{-5} mm^3/N×m, suggesting that, despite the moderate frictional behavior, the wear resistance is compromised due to localized micro-abrasion and reduced mechanical stability [34].

Image J - based dimensional analysis further supports these findings. The groove dimensions were measured as ΔX = 567.72 µm, ΔZ = 0.21 µm along the X-profile, and ΔX = 95.60 µm, ΔZ = 9.65 µm along the Y-profile. The estimated cross-sectional area of the wear groove was 664.40 µm^2, corresponding to a volume of 3.77×10^5 µm^3, lower than the water-quenched counterpart in volume but greater in variability.

These results confirm that oil quenching, while providing some hardening effect, leads to a less controlled wear response under dry sliding conditions.

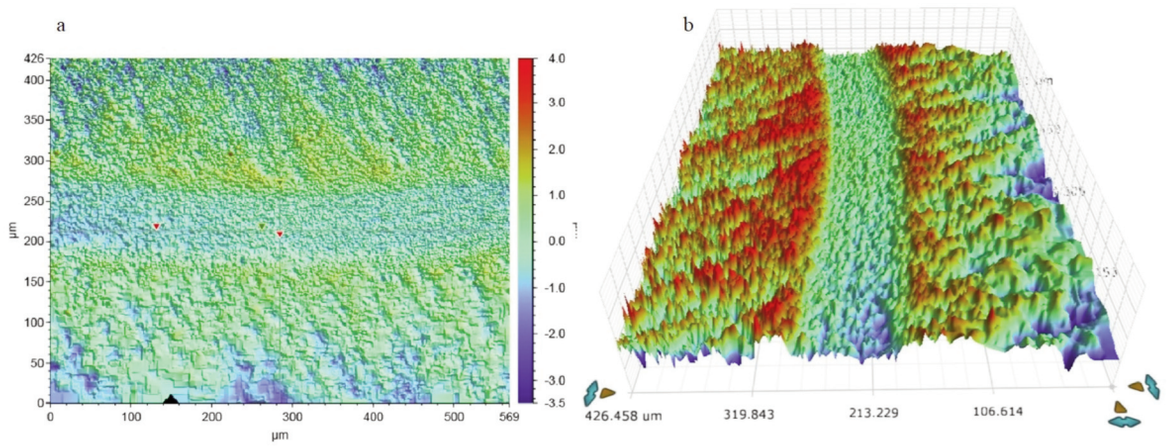

Figure 10. *Surface topography of the wear track on AISI T5 Q-Oil steel after dry sliding test, a) 2D View with Profile b) 3D View with Profiles*

3.3.3.4. Comparative Analysis of Surface Topography and Tribological Performance

When comparing the heat-treated samples, significant differences emerge between the water-quenched and oil-quenched steels in terms of surface morphology and tribological behavior, with the untreated AISI T5 serving as a baseline for comparison. The water-quenched sample exhibited a more uniform and mechanically stable topography, characterized by a lower surface roughness (Ra = 1.60 ± 0.04 µm) and narrow variability across other roughness parameters (Rt = 18.13 ± 0.39 µm, Rv = -9.55 ± 0.21 µm). The consistency in these values suggests a well-controlled martensitic transformation, leading to a high friction coefficient (0.7728) but a significantly reduced wear rate (2.13×10^{-5} $mm^3/N \times m$), indicating improved resistance to material removal under dry sliding.

In contrast, the oil-quenched sample revealed a less homogeneous surface, with greater variability in roughness measurements (Ra = 1.78 ± 0.34 µm, Rt = 17.45 ± 4.10 µm, Rv = -8.74 ± 2.22 µm). This topographical irregularity reflects a less uniform martensitic structure, resulting in a lower friction coefficient (0.7094) with a higher wear rate (4.27×10^{-5} $mm^3/N \times m$) than the water-quenched counterpart. These findings suggest that oil quenching, while partially improving wear resistance compared to the untreated condition, does not provide the same level of structural refinement or abrasion resistance as water quenching.

In summary, although both heat treatments enhance wear performance over the untreated condition, water quenching offers a more effective improvement, delivering superior surface regularity and wear resistance, whereas oil quenching results in more variable surface features and moderately higher wear susceptibility.

3.3.4. Hardness as a Function of Wear rate

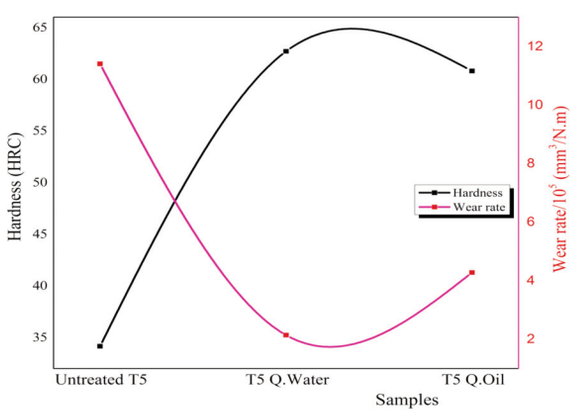

Figure 11. *Hardness as function as wear rate*

The graph in Figure 11 confirms the consistency of the results, highlighting the inverse relationship between hardness and wear rate: a wear rate of 2.13×10^{-5} is observed at 62.7 HRC, compared to 4.27×10^{-5} at 60.8 HRC. This trend aligns with fundamental materials science principles, where higher hardness typically enhances wear resistance. Among the tested conditions, water quenching offers the best compromise, combining the highest surface hardness with the lowest wear rate.

3.4. XRD Analysis

Martensite forms in carbon steels when austenite (γ-Fe), a face-centered cubic solid solution, is rapidly cooled or quenched. This rapid cooling prevents carbon atoms from diffusing out to form cementite, resulting in a transformation to a highly strained, carbon-supersaturated body-centered tetragonal structure. The process generates significant shear deformation and dislocation density, enhancing steel

strength. Transformation begins at the martensite start temperature (Ms) and completes at the finish temperature (Mf). A certain amount of austenite, known as retained austenite, remains after quenching-ranging from negligible levels in low-carbon steels to over 40% in high-carbon steels [35].

For eutectoid steel (~0.78% C), retained austenite typically ranges from 6 to 10 %. Achieving a fully martensitic structure requires extremely rapid quenching to avoid pearlite formation [36].

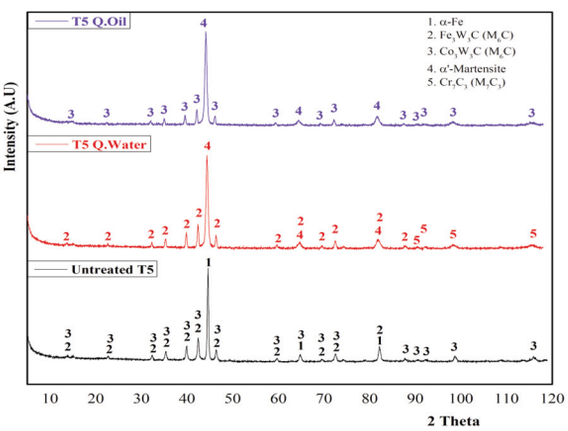

Figure 12. *X-ray diffraction patterns with different treatments*

Although X-ray diffraction (XRD) patterns indicate the presence of the α-phase (ferrite) in both water- and oil-quenched specimens, the signal most likely actually corresponds to martensite. This is due to the fact that martensite exhibits a body-centered tetragonal (bct) structure that closely resembles the body-centered cubic (bcc) structure of ferrite. As a result, distinguishing between these two phases by conventional XRD becomes particularly challenging in steels with moderate carbon content, such as AISI T5. Thus, the α-phase detected in the diffractograms should be interpreted as martensitic in nature.

3.4.1. XRD Analysis of the Untreated AISI T5 Sample

X-ray diffraction (XRD) analysis of the as-received AISI T5 tool steel (Figure 12) revealed the presence of three main crystalline phases: ferrite (α-Fe), tungsten-rich complex carbides of the M_6C type (Fe_3W_3C), and cobalt-tungsten carbides (Co_3W_3C). The matrix is primarily composed of α-Fe with a body-centered cubic (BCC) structure, typical of unquenched high-alloy tool steels at room temperature. The diffraction pattern exhibits strong peaks at 2θ ≈ 44.7°, 65.0°, and 82.3°, corresponding to the (110), (200), and (211) planes of α-Fe, confirming its dominant role as the matrix phase. Additional peaks observed at approximately 40.3°, 46.8°, and 74.2° are attributed to the presence of Fe_3W_3C carbides, while weaker peaks near 35.8° and 60.9° suggest the formation of Co_3W_3C. These carbide phases, which precipitate during solidification and remain stable at room temperature, are distributed both intergranularly and intragranularly within the ferritic matrix. This structural configuration explains the relatively high hardness and wear resistance observed in the as-received condition, as the finely dispersed and stable carbides significantly enhance the mechanical strength and tribological performance of the alloy, even in the absence of any heat treatment [37].

3.4.2. XRD Analysis of the Water-Quenched AISI T5 Sample

The main phase identified through X-ray diffraction (XRD) analysis of AISI T5 steel subjected to water quenching followed by tempering are: α'-Fe (martensitic iron), iron-tungsten carbide Fe_3W_3C (M_6C type), and chromium carbide Cr_7C_3. The α'-Fe phase, corresponding to the tempered martensitic matrix, is identified by its intense diffraction peak at approximately 2θ = 44.6°. The Fe_3W_3C carbide is indicated by characteristic peaks at 2θ ≈ 37.9°, 40.7°, 43.9°, and 62.6°, consistent with its thermal stability and persistence after quenching and tempering. Cr_7C_3 exhibits several peaks between 2θ = 30° and 90°, notably near 36.1°, 59.1°, and 79.3°, suggesting secondary precipitation during tempering - a typical feature of chromium-containing high-speed steels. These chromium carbides precipitate as secondary phases during tempering, contributing to the material's hardness and wear resistance [38]. The Co_3W_3C phase, detected in the untreated condition, is no longer observed, likely due to cobalt dissolution into the matrix at high temperature and its suppression during rapid quenching. In addition, three residual peaks located above 90° (2θ) could not be accounted for by the main identified phases (α'-Fe and Fe_3W_3C). After an extensive database search, only the Cr_7C_3 phase (PDF 03-065-1347) provides a partial match with these reflections. However, the identification score is relatively low (19), and no dominant peaks of this phase are present. Therefore, the presence of Cr_7C_3 in this angular region is proposed as a tentative hypothesis, potentially corresponding to a minor or trace phase, or to structural residuals.

3.4.3. XRD Analysis of the Oil-Quenched AISI T5 Sample

In the case of this quenching medium, XRD analysis of AISI T5 steel reveals the presence of two predominant phases: tempered martensite (α'-Fe) and

the mixed carbide Co_3W_3C. The α'-Fe phase, corresponding to the tempered martensitic matrix, is indicated by a strong diffraction peak at approximately 2θ = 44.6°, typical of the α-Fe structure. The presence of Co_3W_3C is confirmed by several characteristic peaks, notably around 2θ ≈ 31.8°, 36.2°, 40.8°, 52.0°, and 74.0°, reflecting the formation of this metastable cobalt–tungsten carbide phase. Its detection is attributed to the higher austenitization temperature (1200 °C), which promotes greater dissolution of stable carbides such as M_6C and VC, allowing cobalt and tungsten to enter into solid solution. The slower cooling rate of oil quenching (compared to water) enables partial precipitation of Co_3W_3C during cooling in the critical 800–600 °C range. The subsequent tempering at 500 °C stabilizes these precipitates without decomposing them. In contrast, no Fe_3W_3C (M_3C), Cr_7C_3, or VC phases were detected-either due to complete dissolution at high temperature, insufficient re-precipitation kinetics, or low detectability by XRD if finely dispersed or nanocrystalline. Overall, the observed phase evolution is consistent with the thermokinetic conditions of the heat treatment and highlights the role of cooling rate in phase stabilization in high-alloy tool steels.

4. Conclusions

Humidity markedly accelerates AISI T5 oxidation: over two years, the monthly rate reached 11.27×10^{-2} P/P_0 in humid air versus $\leq1.35\times10^{-2}$ P/P_0 in dry air, with cumulative mass gain rising to 2.87×10^{-2} g under humid conditions, while remaining nearly constant in dry air, reflecting protective oxide formation in dry air and moisture-assisted degradation in humid environments.

Heat treatment markedly increased hardness while affecting toughness: Rockwell hardness rose from 34.15 HRC (untreated) to 62.70 HRC (water, 1100 °C) and 60.80 HRC (oil, 1200 °C), while impact toughness decreased to 1.08 Kcv (Q. Water) and 2.08 Kcv (Q. Oil), with oil quenching providing the best hardness-toughness compromise.

Nanoindentation and microhardness confirmed the strengthening sequence: HIT increased from 4.11 GPa (untreated) to 17.39 GPa (Q. Water) and 7.68 GPa (Q. Oil), $HV_{0.5}$ from 381 to 1611 and 711, respectively, while Young's modulus reached 392 GPa (Q. Water) and 222 GPa (Q. Oil), near the untreated 219 GPa, indicating higher stiffness with greater variability after water quenching.

Quenching markedly improved tribological performance: wear rate decreased by 81.3% (Q. Water) and 62.5% (Q. Oil) compared to untreated steel, with steady-state friction coefficients of 0.773 (Q. Water), 0.709 (Q. Oil), and 0.620 (untreated), and a faster run-in for the water quenched surface (~25 s vs. ~200 s for the others).

XRD analysis correlated phase evolution with processing conditions: water quenching produced tempered martensite with Fe_3W_3C and tentative Cr_7C_3, whereas oil quenching resulted in tempered martensite with Co_3W_3C, reflecting the higher austenitizing temperature (1200 °C) and slower cooling rate in oil. These phase differences are consistent with the observed variations in mechanical and tribological properties.

5. Recommendations

Reducing the austenitizing holding time to 15 min. achieved high hardness and wear resistance, with oil quenching providing a balanced toughness, enabling shorter cycle times and lower energy use without compromising performance. For maximum hardness and wear resistance, water quenching at 1100 °C is recommended, while oil quenching at 1200 °C offers the best hardness-toughness balance. A stepwise approach, combining controlled temperature increments and gradual increases in holding time, is suggested to optimize heat treatment. Complementary techniques, such as optical or electron microscopy, are advised alongside XRD to accurately characterize martensite formation.

Acknowledgments

The authors thank the BCL Central Logistics Base of Blida, the CHERAGA Industrial Technologies Research Center and the URMPE Environmental Materials and Processes Research Unit, at the University of Boumerdes.

Conflict of interest

The authors declare that they have no known conflicts of interest.

Author contributions

This work was primarily carried out by the first author, with the others contributing to the validation, revision, structuring, and writing of the manuscript.

Data Availability Statement

Data will be made available on request.

References

[1] R.A. Mesquita, C.A. Barbosa, A.R. Machado, Heat treatment of tool steels, in comprehensive materials finishing (M.S.J. Hashmi, Ed.), Elsevier, Oxford, 2017, p. 214–245.

[2] R.A. Mesquita, Tool Steels: Properties and Performance, CRC Press, Boca Raton, 2016.

[3] M. Seo, D. Kawamata, M. Chiba, Differences in mechanical properties of the passive metal surfaces obtained in solution and air, in passivation of metals and semiconductors, and properties of thin oxide layers, Elsevier Science, Amsterdam, 2006, p. 439–449.

[4] T. Rubben, K. Baert, T. Depover, K. Verbeken, R.I. Revilla, I. De Graeve, Influence of thermal oxide layers on the hydrogen transport through the surface of SAE 1010 Steel, The Journal of The Electrochemical Society, 169 (11) (2022) 111503. https://doi.org/10.1149/1945-7111/aca182

[5] B. Kurt, L. Özdoğan, B. Güney, Ö.S. Bölükbaşı, A. Günen, Characterization and wear behavior of TiBC coatings formed by thermo-reactive diffusion technique on AISI D6 steel, Surface and Coatings Technology, 385 (2020) 125332. https://doi.org/10.1016/j.surfcoat.2020.125332

[6] K. Tankal, B. Güney, M.A. Erden, A comparative study of thermal sprayed Al_2O_3–TiO_2 coatings on PM AISI 316L, Engineering Science and Technology, an International Journal, 60 (2024) 101895. https://doi.org/10.1016/j.jestch.2024.101895

[7] B. Güney, M. Erden, Effect of heat treatments on microstructural and tribological properties of 3D printed 18Ni-300 maraging tool steel made by selective laser sintering process, Science of Sintering, 57 (2024) 26–26. https://doi.org/10.2298/SOS240601026G

[8] M.J. Monteiro, S.R.J. Saunders, F.C. Rizzo, The effect of water vapour on the oxidation of high speed steel, Kinetics and Scale Adhesion, Oxidation of Metals, 75 (1) (2011) 57–76. https://doi.org/10.1007/s11085-010-9220-8

[9] Z. Hou, R.P. Babu, P. Hedström, J. Odqvist, Microstructure evolution during tempering of martensitic Fe-C-Cr alloys at 700 °C, Journal of Materials Science, 53 (9) (2018) 6939–6950. https://doi.org/10.1007/s10853-018-2036-7

[10] Z. Babasafari, M. Motallebzadeh, M. Kazeminezhad, H. R. Abbasi, Effects of austenizing temperature, cooling rate and isothermal temperature on overall phase transformation characteristics in high carbon steel, Journal of Materials Research and Technology, 9 (6) (2020) 15286–15297. https://doi.org/10.1016/j.jmrt.2020.10.071

[11] A. Berger, S. Benito, P. Kronenberg, S. Weber, Impact of thermophysical properties of high-alloy tool steels on their performance in re-purposing applications, Materials (Basel), 15 (23) (2022) 8702. https://doi.org/10.3390/ma15238702

[12] S.K. Saha, L. Prasad, V. Kumar, Experimental investigations on heat Treatment of cold work tool steels: part 1, air-hardening grade (D2), International Journal of Engineering Research and Applications, 2 (2) (2012) 510–519. https://www.ijera.com/pages/v2-no2.html

[13] B. Jiang, M. Wu, M. Zhang, F. Zhao, Z. Zhao, Y. Liu, Microstructural characterization, strengthening and toughening mechanisms of a quenched and tempered steel: Effect of heat treatment parameters, Materials Science and Engineering A, 707 (2017) 306–314. https://doi.org/10.1016/j.msea.2017.09.062

[14] A. Bhateja, A. Varma, A. Kashyap, B. Singh, Study the effect on the hardness of three sample grades of tool steel i.e., EN-31, EN-8, and D3 after heat treatment processes such as annealing, normalizing, and hardening & tempering, International Journal of Engineering Science, 1 (2) (2012) 253–259.

[15] ASTM A 600-92a, Standard specification for tool steel high speed, ASTM International, West Conshohocken, 2004, p. 1–14.

[16] J.E. Bringas, Handbook of comparative world steel standards, 3rd ed., ASTM International, West Conshohocken, 2007, p. 663.

[17] B. Shirley, E. Jarochowska, Chemical characterisation is rough: the impact of topography and measurement parameters on energy-dispersive X-ray spectroscopy in biominerals, Facies, 68 (2) (2022) 7. https://doi.org/10.1007/s10347-022-00645-4

[18] E. Lifshin, R. Gauvin, Precision and detection limits for EDS analysis in the SEM, Microscopy Today, 11 (5) (2003) 46–49. https://doi.org/10.1017/S1551929500053256

[19] W.E. Bryson, Heat treatment: master control manual, Carl Hanser Verlag, Munich, 2015, p. 318.

[20] ISO 14577-1:2015, Metallic materials – Instrumented indentation test for hardness and materials parameters, ISO, Brussels, 2015.

[21] P. Bruckel, P. Lamesle, P. Lours, B. Pieraggi, Isothermal oxidation behaviour of a hot-work tool steel, Materials Science Forum, 461–464 (2004) 831–838. https://doi.org/10.4028/www.scientific.net/MSF.461-464.831

[22] C. Lin, S. Chen, Atmospheric corrosion behavior of mild steel in the initial stage under different relative humidity, International Journal of Georesources and Environment, 4 (2) (2018) 33–39. https://doi.org/10.15273/ijge.2018.02.006

[23] J.H. Mohmmed, Z.I. Al-Hashimy, Effect of different quenching media on microstructure, hardness, and wear behavior of steel used in petroleum industries, Journal of Petroleum Research Studies, 8 (2) (2018) 198–207. https://doi.org/10.52716/jprs.v8i2.244

[24] B.M. Qasim, T.C. Khidir, A.F. Hameed, A.A. Abduljabbar, Influence of heat treatment on the absorbed energy of carbon steel alloys using oil quenching and water quenching, Journal of Mechanical Engineering Research and Developments, 41 (3) (2018) 43–46. http://doi.org/10.26480/jmerd.03.2018.43.46

[25] Y. Wang, R. Wang, W. Yu, Y. Gao, Effect of heat treatment parameters on the modification of nano residual austenite of low-carbon medium-chromium steel, Nanomaterials (Basel, Switzerland), 13 (21) (2023) 2829. https://doi.org/10.3390/nano13212829

[26] M.A. Hafeez, A. Farooq, K. Bin Tayyab, M.A. Arshad, Effect of thermomechanical cyclic quenching and tempering treatments on microstructure, mechanical and electrochemical properties of AISI 1345 steel, International Journal of Minerals, Metallurgy, and Materials, 28 (4) (2021) 688–698. https://doi.org/10.1007/s12613-020-2139-4

[27] K.P. Shaha, Y.T. Pei, D. Martinez-Martinez, J.T.M. De Hosson, Influence of surface roughness on the transfer film formation and frictional behavior of TiC/a-C nanocomposite coatings, Tribology Letters, 41 (1)

(2011) 97–101.
https://doi.org/10.1007/s11249-010-9691-4

[28] X. Han, Z. Zhang, G.C. Barber, S.J. Thrush, X. Li, Wear resistance of medium carbon steel with different microstructures, Materials (Basel), 14 (8) (2021) 2015. https://doi.org/10.3390/ma14082015

[29] O.A. Zambrano, B. Iglesias-Guerrero, S.A. Rodríguez, J.J. Coronado, Running-in period during sliding wear of austenitic steels, Tribology Letters, 72 (3) (2024) 70. https://doi.org/10.1007/s11249-024-01867-z

[30] T.W. Scharf, I.L. Singer, Role of the transfer film on the friction and wear of metal carbide reinforced amorphous carbon coatings during run-in, Tribology Letters, 36 (1) (2009) 43–53. https://doi.org/10.1007/s11249-009-9457-z

[31] B. Wang, M. Zheng, W. Zhang, Analysis and prediction of wear performance of different topography surface, Materials (Basel), 13 (22) (2020) 5056. https://doi.org/10.3390/ma13225056

[32] S. Sackl, G. Kellezi, H. Leitner, H. Clemens, S. Primig, Martensitic transformation of a high-speed tool steel during continuous heat treatment, Materials Today: Proceedings, 2 (2015) S635–S638. https://doi.org/10.1016/j.matpr.2015.07.364

[33] S.M. Arif, H.N. Bar, B.K. Sahoo, C. Chaudhary, D. Mandal, Effect of quench and partitioning treatment on microstructure, tensile Properties, and low cycle fatigue behavior of low-carbon high strength steel, Journal of Materials Engineering and Performance, 34 (2025) 19933–19944. https://doi.org/10.1007/s11665-025-10737-1

[34] G.F. Sun, K. Wang, R. Zhou, A.X. Feng, W. Zhang, Effect of different heat-treatment temperatures on the laser cladded M3:2 high-speed steel, Materials & Design, 65 (2015) 606–616. https://doi.org/10.1016/j.matdes.2014.09.058

[35] J.W.D. Callister, D.G. Rethwisch, Phase transformations in metals, in Materials Science and Engineering: An Introduction, 7th ed., Wiley Publishers, New York, 2007, ch. 10, p. 312–356.

[36] M. Motyka, K. Kubiak, J. Sieniawski, W. Ziaja, Phase transformations and characterization of α + β titanium alloys, in Comprehensive Materials Processing (S. Hashmi, G.F. Batalha, C.J. Van Tyne, B.B. Yilbas, Eds.), Elsevier, Oxford, 2014, pp. 7–36. https://doi.org/10.1016/B978-0-08-096532-1.00202-8

[37] M. Orečný, M. Buršák, M. Šebek, L. Falat, Influence of hardness, matrix and carbides in combination with nitridation on abrasive wear resistance of X210Cr12 tool steel, Metals, 6 (10) (2016) 236. https://doi.org/10.3390/met6100236

[38] Y.-W. Luo, H.-J. Guo, X.-L. Sun, J. Guo, F. Wang, Influence of tempering time on the microstructure and mechanical properties of AISI M42 high-speed steel, Metallurgical and Materials Transactions A, 49 (12) (2018) 5976–5986. https://doi.org/10.1007/s11661-018-4924-5

OKSIDACIJA I EVOLUCIJA SVOJSTAVA ČELIKA AISI T5 POD RAZLIČITIM REŽIMIMA TERMIČKE OBRADE

Abdenour Dadou [a,*], Hamid Dilmi [a] , Boudjema Bezzazi [a], Chouaib Aribi [a,b] , Ismail Daoud [c]

[a] Univerzitet M'hamed Bugara - Bumerdas, Tehnološki fakultet, Alžir
[b] Laboratorija za hranu, preradu, kontrolu i valorizaciju agroresursa, Viša škola za nauku o hrani i prehrambenu industriju, Alžir
[c] Univerzitet za nauku i tehnologiju Huari Bumedien, Laboratorija za nauku i inženjerstvo materijala, Alžir

Apstrakt

Ova studija procenjuje uticaj termičke obrade na mehanička, triboloska i oksidaciona svojstva čelika AISI T5. Hemijski sastav je najpre okarakterisan primenom spektroskopije i SEM-a. Dvogodišnji test oksidacije sproveden u vlažnoj i relativno suvoj atmosferi pokazao je izraženu osetljivost na uslove sredine: u vlažnom vazduhu, brzina oksidacije dostigla je vrednost od $11,27\times10^{-2}$ P/P_0 mesečno sa naglim porastom nakon 25 dana, dok je u suvom vazduhu ostala ispod $1,35\times10^{-2}$ P/P_0 mesečno, prateći linearan i gotovo ravan trend koji ukazuje na zaštitni oksidni sloj. Termička obrada značajno je povećala tvrdoću sa 34,15 ± 0,59 HRC (neobređeni) na 62,70 ± 0,66 i 60,80 ± 0,48 HRC za čelike kaljene u vodi, odnosno ulju. Udarna čvrstoća se proporcionalno smanjila, pri čemu je kaljenje u ulju pružilo najbolji odnos tvrdoće i žilavosti (60,8 HRC, 2,08 Kcv). Instrumentovana indentacija potvrdila je značajno ojačanje površine, sa porastom HIT na 17,39 ± 0,29 GPa (kaljenje u vodi) i 7,68 ± 0,12 GPa (kaljenje u ulju). Pod uslovima suvog klizanja, stope habanja smanjene su za 81,3% (kaljenje u vodi) i 62,5% (kaljenje u ulju), sa bržim početnim habanjem kod kaljenja u vodi. XRD analiza otkrila je otpušteni martenzit sa Fe_3W_3C/Cr_7C_3 (kaljenje u vodi) i Co_3W_3C (kaljenje u ulju), u skladu sa termalnim uslovima. Ova studija pruža nove eksperimentalne podatke o efektima 15-minutne austenitizacije praćene kaljenjem u ulju ili vodi na svojstva čelika AISI T5, ističući njegov potencijal za optimizaciju procesa.

Ključne reči: *AISI T5; Oksidacija; Termička obrada; Tvrdoća; Nanoindentacija; Abrazija*